Limits to the precision of gradient sensing with spatial communication and temporal integration

Andrew Mugler[a,b], Andre Levchenko[c], and Ilya Nemenman[b,d,1]

[a]Department of Physics, Purdue University, West Lafayette, IN 47907; [b]Department of Physics, Emory University, Atlanta, GA 30322; [c]Department of Biomedical Engineering and Yale Systems Biology Institute, Yale University, New Haven, CT 06520; and [d]Department of Biology, Emory University, Atlanta, GA 30322

Edited by Herbert Levine, Rice University, Houston, TX, and approved October 8, 2015 (received for review May 18, 2015)

Gradient sensing requires at least two measurements at different points in space. These measurements must then be communicated to a common location to be compared, which is unavoidably noisy. Although much is known about the limits of measurement precision by cells, the limits placed by the communication are not understood. Motivated by recent experiments, we derive the fundamental limits to the precision of gradient sensing in a multicellular system, accounting for communication and temporal integration. The gradient is estimated by comparing a "local" and a "global" molecular reporter of the external concentration, where the global reporter is exchanged between neighboring cells. Using the fluctuation–dissipation framework, we find, in contrast to the case when communication is ignored, that precision saturates with the number of cells independently of the measurement time duration, because communication establishes a maximum length scale over which sensory information can be reliably conveyed. Surprisingly, we also find that precision is improved if the local reporter is exchanged between cells as well, albeit more slowly than the global reporter. The reason is that whereas exchange of the local reporter weakens the comparison, it decreases the measurement noise. We term such a model "regional excitation–global inhibition." Our results demonstrate that fundamental sensing limits are necessarily sharpened when the need to communicate information is taken into account.

gradient sensing | cell–cell communication | fluctuation–dissipation theorem | linear response theory

Cells sense spatial gradients in environmental chemicals with remarkable precision. A single amoeba, for example, can respond to a difference of roughly 10 attractant molecules between the front and the back of the cell (1). Cells are even more sensitive when they are in a group: Cultures of many neurons respond to chemical gradients equivalent to a difference of only one molecule across an individual neuron's axonal growth cone (2), clusters of malignant lymphocytes have a wider chemotactic sensitivity than single cells (3), and groups of communicating epithelial cells detect gradients that are too weak for a single cell to detect (4). More generally, collective chemosensing properties are often very distinct from those in individual cells (3, 5–7). These observations have generated a renewed interest in the question of what sets the fundamental limit to the precision of gradient sensing in large, spatially extended, often collective sensory systems.

Fundamentally, sensing a stationary gradient requires at least two measurements to be made at different points in space. The precision of these two or more individual measurements bounds the gradient sensing precision (8, 9). In its turn, each individual measurement is limited by the finite number of molecules within the detector volume and the ability of the detector to integrate over time, a point first made by Berg and Purcell (BP) (8). More detailed calculations of gradient sensing by specific geometries of receptors have since confirmed that the precision of gradient sensing remains limited by an expression of the BP type (10–12).

However, absent in this description is the fundamental recognition that for the gradient to be measured, information about multiple spatially separated measurements must be communicated to a common location. This point is particularly evident in the case of multicellular sensing: If two cells at either edge of a population measure concentrations that are different, neither cell "knows" this fact until the information is shared. This is also important for a single cell: Information from receptors on either side of a cell must be transported, e.g., via diffusive messenger molecules, to the location of the molecular machinery that initiates the phenotypic response. How is the precision of gradient sensing affected by this fundamental communication requirement?

As discussed recently in the context of instantaneous measurements (4), the communication imposes important limitations. First, detection of an internal diffusive messenger by cellular machinery introduces its own BP-type limit on gradient sensing. Because the volume of an internal detector must be smaller than that of the whole system, and diffusion in the cytoplasm is often slow, such an intrinsic BP limitation could be dramatic. Second, in addition to the detection noise, the strength of the communication itself may be hampered over long distances by messenger turnover. This imposes a finite length scale over which communication is reliable, with respect to the molecular noise. However, the communicating cells can integrate the signals over time (8), improving detection of even very weak messages. To what extent such integration and the ensuing temporal correlations between the ligand and the communication molecules change the communication constraints has not yet been addressed.

To analyze constraints on gradient sensing in spatially extended systems with temporal integration, we use a minimal model of collective sensing based on the local excitation–global inhibition (LEGI) approach (13). This sensory mechanism uses a

Significance

Knowing which way to move is crucial for many biological processes, from organismal development to migration of cancer cells and from motion of microbes to wound healing. To find their preferred directions, biological systems compare concentrations of a chemical cue at their different edges. The comparison requires information from these different locations to be communicated to the same place. However, all communication is noisy (just think of the childhood game "telephone"). This communication noise, as well as noise in the individual measurements themselves, sets the accuracy of the direction sensing. Here we quantify the importance of the communication noise and propose a mechanism that can improve the accuracy of direction sensing.

Author contributions: A.M., A.L., and I.N. designed research, performed research, analyzed data, and wrote the paper.

The authors declare no conflict of interest.

This article is a PNAS Direct Submission.

[1]To whom correspondence should be addressed. Email: ilya.nemenman@emory.edu.

This article contains supporting information online at www.pnas.org/lookup/suppl/doi:10.1073/pnas.1509597112/-/DCSupplemental.

local and a global internal reporter of the external concentration, where only the global reporter is exchanged and averaged among neighboring cells. Comparison of the two reporters then measures whether the local concentration is above or below the average and hence whether the cell is on the high-concentration edge of the population. We analyze the model, using a fluctuation–dissipation framework (14), to derive the precision with which a chemical gradient can be estimated over long observation times. In the case where the need to communicate is ignored, the precision would grow indefinitely with the number of cells. In contrast, we find that communication imposes limits on sensing even for long measurement times, although slightly different from those on instantaneous sensing (4). Furthermore, the analysis reveals a counterintuitive strategy for optimizing the precision. We find that if the local reporter is also exchanged, at a fraction of the rate of the global reporter, the precision can be significantly enhanced. Even though such exchange makes the two compared concentrations more similar, which weakens the comparison, it reduces the measurement noise of the local reporter. This tradeoff leads to an optimal ratio of exchange rates that maximizes sensory precision. We discuss how our model is realized in classic gradient sensing systems and how its additional predictions could be tested experimentally.

Results

Spatially extended gradient sensors come in different forms, from large spatially extended cells (15, 16) to groups of neighboring cells or nuclei (4, 17–19). We intend to develop a theory that accounts for both structures simultaneously. For this, we view the spatially extended gradient sensor as consisting of compartments. These can be whole cells or their parts, but we refer to them as cells from now on. The limit of a single-cell, homogeneous, spatially extended sensor can be obtained by taking the compartment size to zero, while keeping the overall sensor length constant.

There is a diffusible chemical whose concentration varies linearly in space. The chemical gradient defines a direction within the sensor, and we focus on a chain of cells along this direction (Fig. 1*A*). Numbering the cells from $n=1$ to N, each cell experiences a local concentration $c_n = c_N - (N-n)ag$, where c_N is the background concentration, g is the concentration gradient, and a is the linear size of each cell. We choose without loss of generality to have $g \geq 0$ and to reference the background concentration at cell N, which is then at the higher edge of the gradient. We focus on this cell because we imagine it will be the first to initiate a phenotypic response, such as proliferating or directed motility. Finally, we focus on the limit $ag/c_N \ll 1$ because limits on the sensory precision will be the most important for such small, hard to measure gradients.

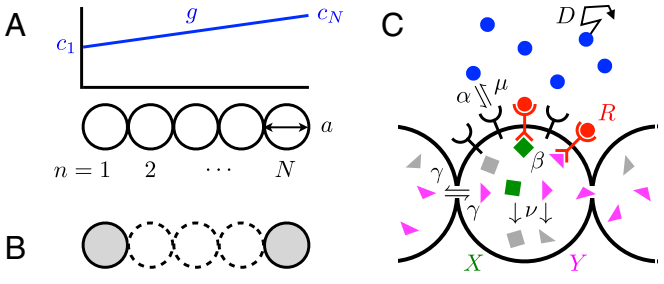

Fig. 1. Spatially extended gradient sensing. (*A*) A chain of N compartments or cells is exposed to a linear profile of a diffusible chemical. (*B*) In an idealized detector, the two edge cells communicate their measurements perfectly and instantly. (*C*) In our model, bound receptors (*R*) activate local (*X*) and global reporter molecules (*Y*), and *Y* is exchanged between cells for the communication. Kinetic rates associated with various processes are indicated by Greek letters.

An Idealized Detector. First, we consider the case when the two edge cells form an idealized detector, in the sense that each cell counts every external molecule in its vicinity and one cell knows instantly and perfectly the count of the other (Fig. 1*B*). The gradient could then be estimated by the difference in the concentration measurements made by the two cells (8, 9). The mean of this difference is $\overline{\Delta} = \bar{c}_N - \bar{c}_1 = (N-1)ag$, and its error is given by the corresponding errors in the two measurements, $(\delta\Delta)^2 = (\delta c_1)^2 + (\delta c_N)^2$, under the assumption that the measurements are independent.

Berg and Purcell (8) showed that the fractional error in each measurement is not smaller than $(\delta c/\bar{c})^2 \sim 1/(aDT\bar{c})$, where D is the diffusion constant of the ligand, and T is the time over which the measurement is integrated. This expression has an intuitive interpretation: The fractional error is at least as large as the Poisson counting noise, which scales inversely with the number of molecular counts. The number of counts that can be made in a time T is given by the number of molecules in the vicinity of a cell at a given time, roughly $\bar{c}a^3$, multiplied by the number of times the diffusion renews these molecules, T/τ, where $\tau \sim a^2/D$. This product is $aDT\bar{c}$.

The error in the gradient estimate is then given by $(\delta\Delta)^2 \sim \bar{c}_1/(aDT) + \bar{c}_N/(aDT)$. For sufficiently small gradients, such that $\bar{c}_1 \approx \bar{c}_N$, this becomes

$$\left(\frac{\delta\Delta}{\bar{c}_N}\right)^2 \sim \frac{1}{aDT\bar{c}_N}. \qquad [1]$$

Thus, for an idealized detector, the error in the gradient estimate is limited entirely by the error in the measurements made by each of the edge cells. In general, we could think of the measurement at either edge being performed by a region that is larger than a single cell. Because each region could not be larger than the whole system, the highest precision is obtained when $\sim Na$ replaces a in Eq. **1**. This result has been derived more rigorously (10), and apart from a constant prefactor, Eq. **1** indeed provides the estimation error in the limit of large detector separation and fast detection kinetics. More complex geometries, such as rings of detectors (10), or detectors distributed over the surface of a circle (11) or a sphere (12), have also been considered, and Eq. **1** again emerges as the corresponding bound, with the length scale a replaced by that dictated by the specific geometry.

Eq. **1** can be combined with the mean $\overline{\Delta}$ to produce the signal-to-noise ratio (SNR) for gradient detection,

$$\frac{1}{\mathrm{SNR}} \equiv \left(\frac{\delta\Delta}{\overline{\Delta}}\right)^2 \sim \frac{\bar{c}_N}{[(N-1)ag]^2 aDT}. \qquad [2]$$

This expression again has a clear interpretation: The SNR increases if the external molecules diffuse more quickly (D) or are more sharply graded (g) or if the detectors are larger (a), are better separated (N), or integrate longer (T). However, the SNR decreases for a larger background concentration ($\bar{c}_N$), because it is more difficult to detect a small gradient on top of a larger background (4). The measures defined in Eqs. **1** and **2** are conceptually equivalent only in the case of low background concentration, when the difference Δ is comparable to the background concentration c_N (i.e., $c_1 \approx 0$). Whereas much of the field has focused on Eq. **1**, here we are concerned with the opposite case: the fundamental limits to the detection of small gradients on a large background. Therefore, from here on we focus on the SNR, Eq. **2**.

Accounting for the Need to Communicate. Eq. **2** cannot be a fundamental limit because it neglects a critical aspect of gradient sensing: the need to communicate information from multiple detectors to a common location. Indeed, the idealized detector implies the existence of a "spooky action at a distance" (20), i.e., an unknown, instantaneous, and error-free communication mechanism. What are the limits to gradient sensing when communication is properly accounted for?

To answer this, a model of gradient sensing must be assumed. A naive model would allow each cell access to information about the input measured and broadcast by every other cell. This would require a number of private communication channels that grow with the number of cells, which is not plausible. A realistic alternative that would involve just one message being communicated is for each cell to have access to some aggregate, average information, to which all comparisons are made. There are a few such models (21–23), and our choice among them is guided by the fact that collective detection of weak gradients is observed in steady state and over a wide range of background concentrations in both neurons (2) and epithelial cells (4). This supports an adaptive spatial (rather than temporal) sensing, such as can be implemented by the local excitation–global inhibition (LEGI) mechanism (13).

The LEGI model is illustrated in Fig. 1*C*. Each cell contains receptors that bind and unbind external molecules with rates α and μ, respectively. Bound receptors (R) activate both a local (X) and a global (Y) intracellular species with rate β. Deactivation of X and Y occurs spontaneously with rate ν. Whereas X is confined to each cell, Y is exchanged between neighboring cells with rate γ, which provides the cell–cell communication. X then excites a downstream species whereas Y inhibits it (LEGI). Conceptually, X measures the local concentration of external molecules, whereas Y represents their spatially averaged concentration. If the local concentration is higher than the average (i.e., the excitation exceeds the inhibition), then the cell is at the higher edge of the gradient. Although such comparison of the excitation and the inhibition can be done by many different molecular mechanisms (13), here we are interested in the limit of shallow gradients. In this limit, biochemical reactions doing the comparison can be linearized around the small difference of X and Y, and the comparison is equivalent to subtracting Y from X (4). Therefore, we take this difference, Δ, as the readout of the model.

Because we are interested in the limits to sensory precision, we focus on the most sensitive regime, the linear response regime, where the effects of saturation are neglected. Introducing r_n, x_n, and y_n as the molecule numbers of R, X, and Y in the nth cell, the stochastic model dynamics are

$$\begin{aligned}
\dot{c} &= D\nabla^2 c - \sum_{n=1}^{N} \delta(\vec{x}-\vec{x}_n)\dot{r}_n,\\
\dot{r}_n &= \alpha c_n - \mu r_n + \eta_n,\\
\dot{x}_n &= \beta r_n - \nu x_n + \xi_n,\\
\dot{y}_n &= \beta r_n - \nu \sum_{n'=1}^{N} M_{nn'} y_{n'} + \chi_n,
\end{aligned} \qquad [3]$$

where $c(\vec{x},t)$ is the external concentration, and $c_n \equiv c(\vec{x}_n,t)$ is the concentration at the location $\vec{x}_n$ of the nth cell. The matrix $M_{nn'} \equiv (1+2\gamma/\nu)\delta_{nn'} - (\gamma/\nu)(\delta_{n',n-1}+\delta_{n',n+1})$ includes the neighbor-to-neighbor exchange terms and is appropriately modified at the endpoints $n \in \{1,N\}$. η_n, ξ_n, and χ_n are the noise terms. Specifically, η_n arises from the equilibrium binding and unbinding of external molecules to receptors and can be expressed in terms of fluctuations in the free energy difference F_n associated with one molecule unbinding from the nth cell (14), $\eta_n = \alpha\bar{c}_n\delta F_n$ (here F_n is in units of the Boltzmann constant times temperature). The Langevin terms ξ_n and χ_n account for noise in the activation, deactivation, and exchange reactions. They have zero mean and obey (24)

$$\begin{aligned}
\langle \xi_n(t)\xi_{n'}(t')\rangle &= \delta_{n'n}(\beta\bar{r}_n + \nu\bar{x}_n)\delta(t-t'),\\
\langle \chi_n(t)\chi_{n'}(t')\rangle &= [\delta_{n'n}(\beta\bar{r}_n + \nu\bar{y}_n + 2\gamma\bar{y}_n + \gamma\bar{y}_{n-1} + \gamma\bar{y}_{n+1})\\
&\quad - \delta_{n',n-1}(\gamma\bar{y}_{n-1} + \gamma\bar{y}_n)\\
&\quad - \delta_{n',n+1}(\gamma\bar{y}_{n+1} + \gamma\bar{y}_n)]\delta(t-t'),
\end{aligned} \qquad [4]$$

where positive terms account for the Poisson noise corresponding to each reaction, and negative terms account for the anticorrelations introduced by the exchange. We are particularly interested in the SNR for the difference between local and global molecule numbers in the edge cell, $\Delta_N = x_N - y_N$, which is the analog of Eq. **2** for the idealized detector.

$\bar{\Delta}$ is given by the means $\bar{x}_N$ and $\bar{y}_N$, which follow from Eq. **3** in steady state: $\bar{x}_N = (\beta/\nu)\bar{r}_N = [\alpha\beta/(\mu\nu)]\bar{c}_N$ and $\bar{y}_N = (\beta/\nu)\sum_n M^{-1}_{Nn}\bar{r}_n = [\alpha\beta/(\mu\nu)]\sum_n M^{-1}_{Nn}\bar{c}_n$, such that

$$\bar{\Delta}_N = \frac{\alpha\beta}{\mu\nu}\left(\bar{c}_N - \sum_{n=0}^{N-1} K_n \bar{c}_{N-n}\right). \qquad [5]$$

Here $K_n \equiv M^{-1}_{N,N-n}$ is the communication "kernel," which determines how neighboring cells' concentration measurements are weighed in producing the global molecule number in the edge cell. Previously we showed (4) that K_n is

$$K_n = \frac{\sum_{j=0}^{N-n-1}\binom{N-n-1+j}{2j}(\nu/\gamma)^j}{\sum_{\ell=0}^{N-1}\binom{N+\ell}{2\ell+1}(\nu/\gamma)^\ell}. \qquad [6]$$

To find the noise, we calculate the power spectra of r, x, and y. As explained below and argued for in Discussion, we assume that the measurement integration time T is longer than the receptor equilibration time (τ_1), the messenger turnover time (τ_2), and the messenger exchange time (τ_3). Under this assumption, (co)variances in long-time averages are given by the low-frequency limits of the power spectra, $C^{xy}_{nn'} = \lim_{\omega\to 0} S^{xy}_{nn'}(\omega)/T$. The first step is to calculate the power spectrum for r_n, which we do using the fluctuation–dissipation theorem (FDT) as in ref. 14. It has been argued (25) that the FDT approach of ref. 14 is inaccurate for a single receptor because it linearizes a binary variable (receptor occupancy) around its mean value. In contrast, here we use the FDT to describe bound receptor number for an entire cell, which can be many thousands. The linear noise approximation is applicable in this case. The FDT relates the power spectrum $S^{rr}_{nn'}(\omega)$ (fluctuations) to the imaginary part of the generalized susceptibility $G_{nn'}(\omega)$ (dissipation),

$$S^{rr}_{nn'}(\omega) = \frac{2}{\omega}\mathrm{Im}[G_{nn'}(\omega)], \qquad [7]$$

where $G_{nn'}(\omega)$ describes how the receptor binding relaxes to small changes in the free energy,

$$\widetilde{\delta r}_n = \sum_{n'} G_{nn'}(\omega)\widetilde{\delta F}_{n'}. \qquad [8]$$

As detailed in *SI Text*, we solve for $G_{nn'}(\omega)$ by linearizing Eq. **3** around its means and Fourier transforming in time and space, which yields a relationship between $\widetilde{\delta r}_n$ and $\widetilde{\delta F}_n$. Writing this relationship in the form of Eq. **8** requires inverting a Toeplitz

marix (a matrix with constant diagonals), which has a known inversion algorithm (26). The result is

$$S^{rr}_{nn'}(\omega) = \frac{2\alpha\bar{c}_{n'}}{\mu^2}\begin{cases}\left(1+\dfrac{\alpha}{2\pi aD}\right) & n'=n,\\ \dfrac{\alpha}{4\pi aD}\dfrac{1}{|n-n'|} & n'\neq n.\end{cases} \quad [9]$$

Here the cell diameter a appears because we cut off the wavevector integrals at the maximal value $k\sim\pi/a$, as in ref. 14. This regularizes unphysical divergences caused by the δ-correlated noises in the Langevin approximation in Eq. **3**. In deriving Eq. **9**, we have made the first of our timescale assumptions, namely $T\gg\tau_1\equiv\mu^{-1}+K/4\pi\sigma D$, where $K\equiv\alpha/\mu$ is the equilibrium constant, and $\sigma\equiv a/2$ is the cell radius. τ_1 is the receptor equilibration timescale: It is the time it takes for a signal molecule to unbind from the receptors and diffuse away from the cell into the bulk (27). Its first term is the intrinsic receptor unbinding time, and its second term accounts for rebinding events before the molecule diffuses far away (25).

The second step is to calculate power spectra for x_N and y_N. As shown in *SI Text*, we calculate these directly from the Fourier transform of Eq. **3** and the noise correlations in Eq. **4**, which propagate via the same matrix $M_{nn'}$ as the means (28). The result is an expression for the variance $(\delta\Delta_N)^2=(\delta x_N)^2+(\delta y_N)^2-2C^{xy}_{NN}=[S^{xx}_{NN}(0)+S^{yy}_{NN}(0)-2S^{xy}_{NN}(0)]/T$, namely

$$(\delta\Delta_N)^2=\frac{\beta^2}{\nu^2}\left[\frac{S^{rr}_{NN}(0)}{T}+\sum_{nn'}K_{N-n}K_{N-n'}\frac{S^{rr}_{nn'}(0)}{T}-2\sum_n K_{N-n}\frac{S^{rr}_{Nn}(0)}{T}\right]+\frac{2}{\nu T}(\bar{x}_N+K_0\bar{y}_N). \quad [10]$$

Eqs. **5** and **10**, together with Eqs. **6** and **9**, give the SNR $=(\overline{\Delta}_N/\delta\Delta_N)^2$, which we do not write here for brevity. In taking the low-frequency limit to obtain Eq. **10**, we have made our second timescale assumption, namely $T\gg\tau_2\equiv 1/\nu$, where τ_2 is the timescale of messenger turnover by degradation.

The SNR is compared with the result for the idealized detector (Eq. **2**) in Fig. 2. We see that whereas the SNR for the idealized detector increases indefinitely with the number of cells N, the SNR for the model with communication and temporal integration saturates, as in the no-integration case (4). This is our first main finding: Communication leads to a maximum precision of gradient sensing, which a multicellular system cannot surpass no matter how large it grows. The reason is that communication is not infinitely precise over large length scales. In the next section, we make this point clear by deriving a simple fundamental expression for the maximum value of the SNR.

Fundamental Limit to Sensory Precision. Our results up to this point hold for arbitrary communication strengths and cell numbers and are applicable to multicellular systems or cellular compartments. However, it is instructive to derive the saturating value of the SNR in the limit of large N and strong communication, where messenger hopping between cells is equivalent to continuous diffusion. In this limit, and when communication is strong ($\gamma\gg\nu$), the kernel (Eq. **6**) reduces to $K(n,n_0)\approx e^{-n/n_0}/n_0$ (4). Here $n_0\equiv\sqrt{\gamma/\nu}$ sets the length scale of the kernel and therefore sets the number of neighboring cells with which the edge cell effectively communicates. The limit $\gamma\gg\nu$ and our assumption $T\gg\tau_2=1/\nu$ imply our third timescale assumption, $T\gg\tau_3\equiv 1/\gamma$, i.e., that the integration time is longer than the timescale of messenger exchange from cell to cell. Inserting the expression for $K(n,n_0)$ into Eq. **5** and approximating the sum as an integral in the large

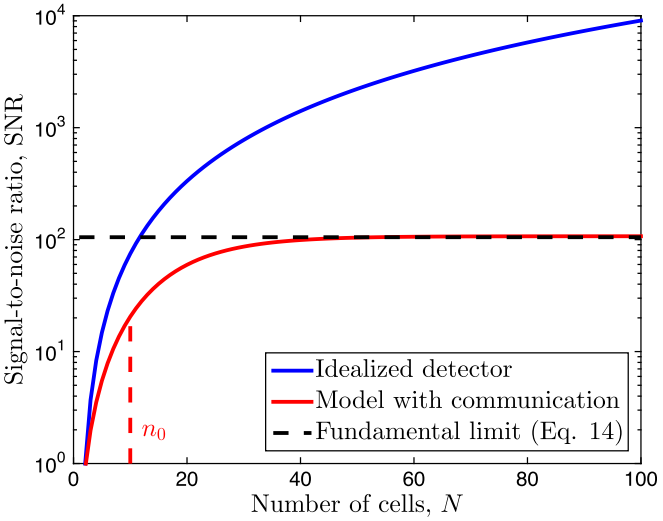

Fig. 2. Precision of gradient sensing with temporal integration. Signal-to-noise ratio (SNR) vs. number of cells N is shown for the idealized detector (Eq. **2** with prefactor $1/\pi$) and for our model with communication (Eqs. **5**, **6**, **9**, and **10**). Whereas the SNR for the idealized detector increases indefinitely, the SNR for the model with communication saturates for $N\gg n_0$. The saturation level is bounded from above by the fundamental limit, Eq. **11**. As shown, the bound is reached in the high-gain regime $\alpha/a^3\mu=\beta/\nu=100$, where intrinsic noise is negligible. Other parameters are $a=10$ μm, $\bar{c}_N=1$ nM, $g=1$ nM/mm, $D=50$ μm^2/s, $\mu=\nu=1$ s^{-1}, and $n_0=\sqrt{\gamma/\nu}=10$, and the integration timescale is $T=10$ s.

N limit, the mean becomes $\overline{\Delta}_N\approx(\alpha\beta/\mu\nu)(\bar{c}_N-\bar{c}_{N-n_0})=\alpha\beta n_0 ag/\mu\nu$. Inserting $K(n,n_0)$ into Eq. **10** results in products of the exponential with the $1/|n-n'|$ dependence of the bound receptor power spectrum (Eq. **9**), leading to sums like $\sum_j e^{-j}/j$, which we evaluate in *SI Text*. The result is

$$\frac{1}{\mathrm{SNR}}=\left(\frac{\delta\Delta_N}{\overline{\Delta}_N}\right)^2\gtrsim\frac{c_{\mathrm{eff}}}{\pi(n_0 ag)^2 aDT}, \quad [11]$$

where

$$c_{\mathrm{eff}}\equiv\bar{c}_N+\frac{\log n_0}{2n_0}\left(\bar{c}_{N-n_0/2}-2\bar{c}_N\right), \quad [12]$$

and $T\gg\{\tau_1,\tau_2,\tau_3\}$. Eq. **11** is fundamental in the sense that it does not depend on the details of the internal sensory mechanism. Rather, it depends only on the properties of the external signal (c,g,D), the physical dimensions (a), and the fact that information is integrated (T) and communicated (n_0) by the cells. The inequality reflects the fact that the right-hand side contains additional positive terms arising from the finite number of bound receptors and intracellular molecules (*SI Text*). These terms represent intrinsic noise and can in principle be made arbitrarily small by increasing the gain factors $\alpha/a^3\mu$ and β/ν, which dictate the internal molecule numbers. What remains in Eq. **11** is the communicated extrinsic noise, which arises unavoidably from the diffusive fluctuations in the numbers of the ligand molecules being detected. Eq. **11** is shown to bound the exact SNR in Fig. 2.

Comparing Eq. **11** to the expression for the idealized detector (Eq. **2**), we see that the expressions are very similar but contain two important differences. First, whereas Eq. **2** decreases indefinitely with N, Eq. **11** remains bounded by n_0 for large N (Fig. 2). Evidently, a very large detector is limited in its precision to that of a smaller detector with effective size n_0. This limitation reflects the fact that reliable communication is restricted to a

finite length scale. Importantly, Eq. **11** demonstrates that this noise is present independently of the number of intrinsic signaling molecules in the communication channel. Thus, the fundamental sensory limit is affected not only by the measurement process (as in BP theory), but also unavoidably by the communication process.

The second important difference is that Eq. **2** depends on $\bar{c}_N$, whereas Eq. **11** depends on the effective concentration c_{eff}, defined in Eq. **12**. c_{eff} is a sum of the concentration measured by the local species, the global species, and the covariance between them, respectively. The local species measures the concentration only within its local vicinity, $\bar{c}_N$. However, the global species effectively measures the concentration in the vicinity of n_0 cells. This fact reduces the noise associated with this term (and the covariance term) by the factor of n_0 in the denominator of Eq. **12**. Because intercellular molecular exchange also competes with extracellular molecular diffusion, not all of the measurements made by these n_0 cells are independent. Therefore, the reduction is tempered by the $\log n_0$ factor in the numerator of Eq. **12**. This log arises from the interaction of the e^{-n} exchange kernel with the $1/|n-n'|$ diffusion kernel (*SI Text*). The net result is that, because of the correlations imposed by external diffusion, the number of independent measurements grows sublinearly with the system size. For real biological systems n_0 is small (4, 19), such as $n_0 \approx 4$ for mammary epithelial organoids. However, as shown in *SI Text*, the asymptotic expansion in Eqs. **11** and **12** is still very accurate in this range. Thus, this logarithmic correction cannot be summarily neglected. Nonetheless, even with the correction, in Eq. **12** the measurement noise in the global species decreases with the communication length scale n_0. Crucially, this means that Eq. **11** is dominated by the measurement noise of the local species, i.e., the first term in Eq. **12**.

In deriving the precision of gradient sensing, we have also derived the precision of concentration sensing by communicating cells. Specifically, by focusing only on the global species terms, and following the steps leading to Eq. **11**, we get

$$\left(\frac{\delta y_N}{\bar{y}_N}\right)^2 \gtrsim \frac{1}{2\pi a_{\text{eff}} DTc_{\text{eff}}}, \qquad [13]$$

where $a_{\text{eff}} \equiv an_0/\log n_0$ and $c_{\text{eff}} \equiv \bar{c}^2_{N-n_0}/\bar{c}_{N-n_0/2}$. This expression has the same form as the BP limit, $(\delta c/\bar{c})^2 \sim 1/(aDT\bar{c})$. Indeed, in the absence of a gradient, $\bar{c}_n = \bar{c}_N$ is constant, and $c_{\text{eff}} \to \bar{c}_N$. Importantly, however, the effect of communication remains present in a_{eff}: Messenger exchange expands the effective detection length scale by a factor n_0, whereas ligand diffusion once again tempers the expansion by $\log n_0$, which is an important correction if n_0 is not too large. The net result is that communication reduces error by increasing the effective detector size, $a_{\text{eff}} > a$. Note that previous analyses that considered effects of spatial averaging on concentration sensing accuracy did not consider either communication noise (29) or effects of correlations between messenger concentrations in different detector compartments induced by the ligand diffusion (17, 19), resulting in expressions different from Eq. **13**.

Optimal Sensing Strategy. In the previous section, we saw that the limit to the precision of multicellular gradient sensing is dominated by the measurement noise of the local species in the edge cell (Eqs. **11** and **12**). In contrast, the measurement noise of the global species is reduced by the intercellular communication. This finding raises an interesting question: Could the total noise be further reduced if the local species were also exchanged between cells? To explore this possibility, we extend the model in Eqs. **3** and **4** to allow for exchange of the local species at rate γ_x, and we take $\gamma \to \gamma_y > \gamma_x$ for the global species. An immediate consequence of this modification is that the signal becomes $\overline{\Delta}_N \approx \alpha\beta(n_y - n_x)ag/\mu\nu$, where $n_x \equiv \gamma_x/\nu$ and $n_y = \gamma_y/\nu$. Thus, the signal is reduced by local exchange, because increasing γ_x decreases the difference $n_y - n_x$. This is because the signal is defined by the difference between the global and local readouts, and allowing for the local species exchange makes the two readouts less different. We thus anticipate that any useful local exchange rate will satisfy $\gamma_x \ll \gamma_y$ to maintain sufficiently high signal. In this limit, we find that Eq. **12** remains dominated by the first term, even as local exchange reduces this term according to $c_N \to \bar{c}_N(\log n_x)/2n_x$. Eq. **11** then becomes

$$\text{SNR} \lesssim \frac{2\pi(ag)^2 aDT}{\bar{c}_N} \frac{(n_y - n_x)^2 n_x}{\log n_x}. \qquad [14]$$

For large n_y, this expression has a maximum as a function of n_x. The maximum arises due to a fundamental tradeoff: Exchange of the local species reduces the signal, but it also reduces the dominant local measurement noise.

The optimal value n_x^* depends on n_y. Experiments in epithelial cells suggest that the communication length scale n_y is on the order of a few cells (4). In this range, we find the optimum numerically from the exact SNR, which comes from straightforwardly generalizing Eq. **10** (Eq. **S67** in *SI Text*). Fig. 3 shows that n_x^* is about half of n_y for one specific set of parameters, leading to an optimal exchange rate ratio of $\gamma_x^*/\gamma_y = (n_x^*/n_y)^2 \approx 25\%$. Although the exact optimal ratio depends on the relative strengths of different noises, and hence on the gains (Fig. S1), the main finding is robust: A multicellular system should exchange both antagonistic messenger molecules, one at a fraction of the rate of the other. We call this strategy "regional excitation–global inhibition" (REGI). Fig. 3 shows that the enhancement over the one-messenger LEGI strategy can be substantial. For example, with $n_y = 10$ cells, the SNR is optimally enhanced by a factor of 5. With $n_y = 15$, the enhancement is almost eightfold.

Discussion

Cellular sensing of spatially inhomogeneous concentrations is a fundamental biological computation, involved in a variety of

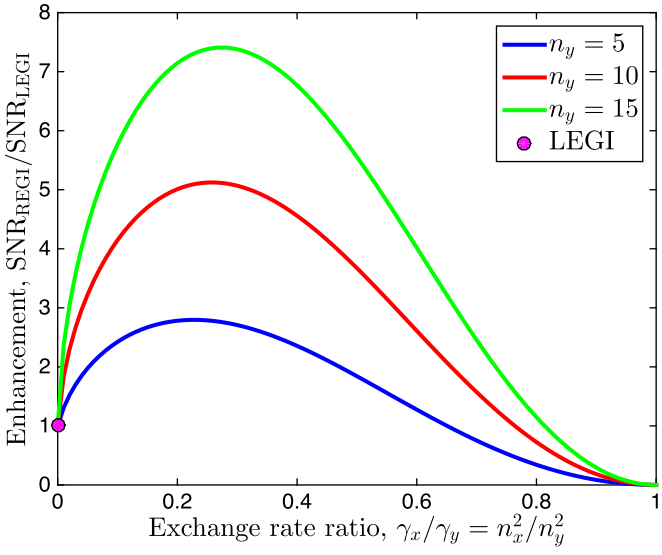

Fig. 3. Regional excitation–global inhibition (REGI). Signal-to-noise ratio (SNR) is enhanced by allowing both messengers to be exchanged between cells. The optimal enhancement over LEGI is substantial and occurs because exchange of the local species reduces measurement noise, but also reduces the signal. Parameters are as in Fig. 2, but with $N = 100$, $\alpha/a^3\mu = \beta/\nu = 5$, and several values of $n_y \equiv \sqrt{\gamma_y/\nu}$ as indicated.

processes in the development and behavior of living systems. Like binocular vision and stereophonic sound processing, it is a process where the sensing is done by an array of spatially distributed sensors. Thus, the accuracy of sensing is limited in part by the physical properties of the biological machinery that brings together the many spatially distributed measurements. Understanding these limits is a difficult problem.

Here we solved this problem in the case where the communication is diffusive, and one-dimensional distributed measurements are used to calculate external concentration gradients within the LEGI paradigm. We allowed for temporal integration, extending the results of ref. 4. Some of the features of the gradient sensing limit we derived (Eq. **11**), such as the unbounded increase of the SNR with the diffusion coefficient of the ligand or with the integration time, carry over from the Berg–Purcell theory of gradient sensing (12), which does not account for communication. However, our most important finding is that, in contrast to the BP theory, the growth of the sensor array beyond a certain size stops increasing the SNR. The effect is independent of the intrinsic noise in the communication system and thus represents a truly fundamental limitation of diffusive communication for distributed sensing. In particular, it holds for multicellular systems, as well as for large individual cells. Although we derived the limit for a linear signal profile, we anticipate that the limit for a nonlinear profile will be similar, Eq. **11**, but with a different effective concentration c_{eff}. It remains to be seen whether similar limits hold when the sensors are arranged in 2D or 3D structures or when concentration information propagates superdiffusively, as is possible in wave-based or Turing-type models of polarization establishment (23). Additionally, it will be important to relax various assumptions of the model, such as allowing for saturation of receptors or limiting the total number of messengers and coupling the model to the motility apparatus to investigate how the improved sensory precision affects downstream functions.

Our results illustrate two important features of temporal averaging by distributed sensors. First, our derivation naturally reveals which timescales are relevant in this process, namely receptor equilibration ($\tau_1 = \mu^{-1} + K/4\pi\sigma D$), messenger turnover ($\tau_2 = 1/\nu$), and messenger exchange ($\tau_3 = 1/\gamma$), which was unclear in simpler previous analyses. In principle, these timescales could have depended on system-level properties, such as the system size (N) or the communication length (n_0). Surprisingly, instead they depend only on single-cell properties, meaning that efficient temporal averaging is not slowed down by increasing the number of sensors. Second, our results reveal the effects of overcounting due to correlations between external and internal diffusion. In both gradient sensing (Eqs. **11** and **12**) and concentration sensing (Eq. **13**), we see that the noise reduction afforded by communication-based averaging is tempered by a factor $\log n_0$. This log is not a mathematical curiosity. Rather, it reflects the fact that not all measurements communicated to a cell by its neighbors are independent because the signal molecules also diffuse externally. Coupling external diffusion with internal exchange introduces correlations among measurements, which reduces the benefit of internal averaging. This effect has been omitted in previous analyses of concentration sensing by extended systems (17, 19). At the same time, for multicellular mammary organoids (4), n_0 is estimated as ~ 4, so that $\log n_0$ is not much smaller than n_0 itself and should not be neglected.

Our analysis of the limits on the gradient sensing accuracy has assumed that the integration time is longer than any of the other timescales in the problem, $T \gg \{\tau_1, \tau_2, \tau_3\}$ (receptor equilibration, messenger turnover, and messenger exchange). It is crucial to understand whether such an assumption is experimentally relevant. First, in *Dictyostelium*, $a \sim 1$ μm is a typical size of an initial membrane protrusion, which can be viewed as a minimal sensing unit. The dissociation constant of cAMP is $K_{\text{d}} = K^{-1} \approx 0.2$ μM, its dissociation rate is $\mu \approx 1\ \text{s}^{-1}$, and cAMP diffusion constant is $D \approx 400\ \mu\text{m}^2\ \text{s}^{-1}$ (30). Thus, $\tau_1 \approx 1$ s. The identity of the diffusive messenger is still being debated, although some suggest it is RasGAP, a 120-kDa protein (31). Although its cytosolic turnover rate and the diffusion constant are unknown, the estimates are $\nu \sim \gamma \sim 1\ \text{s}^{-1}$ (30, 32). The onset of the *Dictyostelium* gradient response takes about 30 s, and the adaptation phase (global inhibition) can be 300 s or longer (16). This validates our assumptions that T can be much larger than any of τ_i, allowing for temporal integration. Interestingly, ref. 12 shows that the integration actually occurs, and they estimate $T \approx 3.2$ s. This is already longer than each of τ_i and can also be seen as an underestimate because their analysis neglected noise in communication and further downstream of sensing, which would decrease SNR and reduce the apparent integration time.

Similar analysis can be done for multicellular sensors, such as EGF gradient sensing by mammary epithelial organoids in the companion paper (4). There the ligand is EGF, and the messenger is associated with calcium signaling and is able to pass through gap junctions; one possibility is inositol 1,4,5-trisphosphate (IP3). The cell size is $a \sim 10$ μm, the dissociation constant is as small as $K_{\text{d}} = K^{-1} \sim 200$ pM (33), the dissociation rate is $\mu \sim 0.001\ \text{s}^{-1}$ (34), and the EGF diffusion constant is $D \sim 50\ \mu\text{m}^2\ \text{s}^{-1}$ (35). The turnover rate of IP3 is estimated as $\nu \sim 0.1\ \text{s}^{-1}$ (36). Thus, $\tau_1 \sim 15$ min, $\tau_2 \sim 10$ s, and the exchange time of IP3 among cells is $\tau_3 \sim 1$ s (37) (it is slower than the diffusion in the cytoplasm would allow due to bottlenecks at gap junctions). In contrast, the response in this system is measured on the scales of hours or days (4), allowing for temporal integration and validating our timescales assumptions, $T \gg \{\tau_1, \tau_2, \tau_3\}$. These arguments make it clear that the timescales of these systems warrant the approximations we make, although whether the time integration is actually used may vary by organism.

Another central prediction of our theory is that the gradient sensing is improved by a system with two messengers, exchanged at different rates. We call this mechanism REGI, a generalization of the standard LEGI model. Optimality of REGI follows directly from the interplay between the ligand stochasticity and the communication constraints. Therefore, REGI has not been identified as an optimal strategy in previous studies that neglected either of these two effects. Although the need for spatial averaging of two measurements involved in gradient detection was proposed (38), no model of the communication was suggested, limiting the ability of that analysis to make specific predictions.

Molecular mechanisms supporting REGI are suggested by biophysical mechanisms in many eukaryotic cell types. There activated receptor complexes, which diffuse in the membrane at the rate of $\sim 10-100$ times slower than similarly sized cytosolic molecules (32), could act as the regional messengers. Further, the initial size of protrusions in the cell membrane of a migrating *Dictyostelium* cell is a few microns in size, which is a sizable fraction of a cell size of about 10–20 μm. These can be identified with regionally averaging functional units in our terminology. Diffusion of surface receptors and finite membrane rigidity ensure the existence of regional integration in other eukaryotic cells, further supporting REGI over LEGI as a correct model.

REGI emerged from maximizing the SNR in our system, which revealed the optimal rate ratio γ_x/γ_y. Maximization of the SNR also implies that the optimal value of γ_y (or n_y) is infinity, because the SNR grows indefinitely with n_y (Fig. 3). Infinite n_y corresponds to averaging over as large a distance as possible. Such a strategy is optimal here only because the concentration profile is linear, with constant gradient g. In contrast, more physical nonlinear profiles (e.g., exponential, power law, randomly varying, or profiles with extrema) have spatially varying g. In these cases, if the size of the group of cells is larger than the correlation length of g, then an infinite n_y would average out the signal

together with the noise, which would reduce the SNR. In contrast, a finite n_y would allow a subset of cells to detect the local gradient in their vicinity, which is an essential task in morphological processes such as tissue branching and collective migration.

REGI can be interpreted as performing a spatial derivative. Specifically, the two-lobed filter $K(n,n_x)-K(n,n_y)$ reports the difference in concentrations measured over distances n_x and n_y near a given detector, and the values n_x and n_y depend on the properties of the environment. Thus, REGI is similar to the temporal differentiation in *Escherichia coli* chemotaxis. Indeed, the temporal filter of the *E. coli* sensory module is also two-lobed, with the short and long timescales set by ligand statistics and rotational diffusion, respectively (39). Thus, for both spatial and temporal filtering, the choice of the two optimal length scales or timescales is determined by matching the filter to the statistical properties of the signal and the noise (40), which is understood well for *E. coli* (39).

Interpreting the REGI model as a spatiotemporal filter suggests experiments that would identify whether a certain biological system employs this mechanism. Such experiments would involve concentration profiles that differ substantially from steady-state linear gradients. For example, subjecting cells to a concentration profile with a spatially localized maximum would allow one to measure both γ_x and γ_y by observing the response of cells near the concentration peak as a function of the peak width. Alternatively, one can subject cells to a spatiotemporally localized concentration pulse and observe whether a response a certain distance away from the pulse exhibits the signs of only inhibition (LEGI, one messenger) or inhibition and excitation on different scales (REGI, two messengers). Understanding fundamental sensory limits for diffusive communication in gradient sensing opens up possibilities to propose and analyze these and other related experiments.

ACKNOWLEDGMENTS. We thank Matt Brennan for useful discussions and Thomas Sokolowski for pointing out a more rigorous way to derive the $\log n_0$ factor. A.M. and I.N. were supported in part by the James S. McDonnell Foundation Grant 220020321 and the Human Frontiers Science Program Grant RGY0084/2011. I.N. was further supported by the National Science Foundation (NSF) Grant PoLS-1410978. A.L. was supported in part by National Institutes of Health Grants CA155758 and GM072024, by NSF Grant PoLS-1410545, and by the Semiconductor Research Corporation's SemiSynBio program.

1. Song L, et al. (2006) Dictyostelium discoideum chemotaxis: Threshold for directed motion. *Eur J Cell Biol* 85(9–10):981–989.
2. Rosoff WJ, et al. (2004) A new chemotaxis assay shows the extreme sensitivity of axons to molecular gradients. *Nat Neurosci* 7(6):678–682.
3. Malet-Engra G, et al. (2015) Collective cell motility promotes chemotactic prowess and resistance to chemorepulsion. *Curr Biol* 25(2):242–250.
4. Ellison D, et al. (2015) Cell-cell communication enhances the capacity of cell ensembles to sense shallow gradients during morphogenesis. *arXiv:*1508.04692.
5. Friedl P, Gilmour D (2009) Collective cell migration in morphogenesis, regeneration and cancer. *Nat Rev Mol Cell Biol* 10(7):445–457.
6. Donà E, et al. (2013) Directional tissue migration through a self-generated chemokine gradient. *Nature* 503(7475):285–289.
7. Pocha SM, Montell DJ (2014) Cellular and molecular mechanisms of single and collective cell migrations in Drosophila: Themes and variations. *Annu Rev Genet* 48:295–318.
8. Berg HC, Purcell EM (1977) Physics of chemoreception. *Biophys J* 20(2):193–219.
9. Goodhill GJ, Urbach JS (1999) Theoretical analysis of gradient detection by growth cones. *J Neurobiol* 41(2):230–241.
10. Endres RG, Wingreen NS (2009) Accuracy of direct gradient sensing by cell-surface receptors. *Prog Biophys Mol Biol* 100(1–3):33–39.
11. Hu B, Chen W, Rappel WJ, Levine H (2010) Physical limits on cellular sensing of spatial gradients. *Phys Rev Lett* 105(4):048104.
12. Endres RG, Wingreen NS (2008) Accuracy of direct gradient sensing by single cells. *Proc Natl Acad Sci USA* 105(41):15749–15754.
13. Levchenko A, Iglesias PA (2002) Models of eukaryotic gradient sensing: Application to chemotaxis of amoebae and neutrophils. *Biophys J* 82(1 Pt 1):50–63.
14. Bialek W, Setayeshgar S (2005) Physical limits to biochemical signaling. *Proc Natl Acad Sci USA* 102(29):10040–10045.
15. Paliwal S, et al. (2007) MAPK-mediated bimodal gene expression and adaptive gradient sensing in yeast. *Nature* 446(7131):46–51.
16. Wang CJ, Bergmann A, Lin B, Kim K, Levchenko A (2012) Diverse sensitivity thresholds in dynamic signaling responses by social amoebae. *Sci Signal* 5(213):ra17.
17. Erdmann T, Howard M, ten Wolde PR (2009) Role of spatial averaging in the precision of gene expression patterns. *Phys Rev Lett* 103(25):258101.
18. Lander AD (2011) Pattern, growth, and control. *Cell* 144(6):955–969.
19. Sokolowski TR, Tkačik G (2015) Optimizing information flow in small genetic networks. IV. Spatial coupling. *Phys Rev E Stat Nonlin Soft Matter Phys* 91(6):062710.
20. Mermin N (1985) Is the moon there when nobody looks? Reality and the quantum theory. *Phys Today* 38(4):38–47.
21. Meinhardt H (1999) Orientation of chemotactic cells and growth cones: Models and mechanisms. *J Cell Sci* 112(Pt 17):2867–2874.
22. Rappel WJ, Thomas PJ, Levine H, Loomis WF (2002) Establishing direction during chemotaxis in eukaryotic cells. *Biophys J* 83(3):1361–1367.
23. Jilkine A, Edelstein-Keshet L (2011) A comparison of mathematical models for polarization of single eukaryotic cells in response to guided cues. *PLoS Comput Biol* 7(4):e1001121.
24. Gillespie DT (2007) Stochastic simulation of chemical kinetics. *Annu Rev Phys Chem* 58:35–55.
25. Kaizu K, et al. (2014) The Berg-Purcell limit revisited. *Biophys J* 106(4):976–985.
26. Zohar S (1969) Toeplitz matrix inversion: The algorithm of WF Trench. *J Assoc Comput Mach* 16:592–601.
27. Agmon N, Szabo A (1990) Theory of reversible diffusion-influenced reactions. *J Chem Phys* 92:5270–5284.
28. Detwiler PB, Ramanathan S, Sengupta A, Shraiman BI (2000) Engineering aspects of enzymatic signal transduction: Photoreceptors in the retina. *Biophys J* 79(6):2801–2817.
29. Gregor T, Tank DW, Wieschaus EF, Bialek W (2007) Probing the limits to positional information. *Cell* 130(1):153–164.
30. Ueda M, Shibata T (2007) Stochastic signal processing and transduction in chemotactic response of eukaryotic cells. *Biophys J* 93(1):11–20.
31. Takeda K, et al. (2012) Incoherent feedforward control governs adaptation of activated ras in a eukaryotic chemotaxis pathway. *Sci Signal* 5(205):ra2.
32. Kholodenko BN, Hoek JB, Westerhoff HV (2000) Why cytoplasmic signalling proteins should be recruited to cell membranes. *Trends Cell Biol* 10(5):173–178.
33. Björkelund H, Gedda L, Andersson K (2011) Comparing the epidermal growth factor interaction with four different cell lines: Intriguing effects imply strong dependency of cellular context. *PLoS One* 6(1):e16536.
34. Zhou M, et al. (1993) Real-time measurements of kinetics of EGF binding to soluble EGF receptor monomers and dimers support the dimerization model for receptor activation. *Biochemistry* 32(32):8193–8198.
35. Thorne RG, Hrabetová S, Nicholson C (2004) Diffusion of epidermal growth factor in rat brain extracellular space measured by integrative optical imaging. *J Neurophysiol* 92(6):3471–3481.
36. Wang SS, Alousi AA, Thompson SH (1995) The lifetime of inositol 1,4,5-trisphosphate in single cells. *J Gen Physiol* 105(1):149–171.
37. Decrock E, et al. (2013) IP3, a small molecule with a powerful message. *Biochim Biophys Acta* 1833(7):1772–1786.
38. Xu J, Rosoff WJ, Urbach JS, Goodhill GJ (2005) Adaptation is not required to explain the long-term response of axons to molecular gradients. *Development* 132(20):4545–4552.
39. Berg HC (2004) *E. Coli in Motion* (Springer, New York).
40. Wiener N (1964) *Extrapolation, Interpolation, and Smoothing of Stationary Time Series: With Engineering Applications* (MIT Press, Cambridge, MA).

Supporting Information

Mugler et al. 10.1073/pnas.1509597112

SI Text

Derivation of the Power Spectra

Linearizing Eq. **3** of the main text around its means and Fourier transforming (denoted by ~) in time and space obtains

$$-i\omega\widetilde{\delta c} = -Dk^2\widetilde{\delta c} + i\omega\sum_n \widetilde{\delta r}_n\, e^{i\vec{k}\cdot\vec{x}_n}, \quad \text{[S1]}$$

$$-i\omega\widetilde{\delta r}_n = \alpha\widehat{\delta c}\left(\vec{x}_n,\omega\right) - \mu\widetilde{\delta r}_n + \alpha\bar{c}_n\widetilde{\delta F}_n, \quad \text{[S2]}$$

$$-i\omega\widetilde{\delta x}_n = \beta\widetilde{\delta r}_n - \nu\widetilde{\delta x}_n + \tilde{\xi}_n, \quad \text{[S3]}$$

$$-i\omega\widetilde{\delta y}_n = \beta\widetilde{\delta r}_n - \nu\sum_{n'} M_{nn'}\widetilde{\delta y}_{n'} + \tilde{\chi}_n, \quad \text{[S4]}$$

where

$$\widehat{\delta c}\left(\vec{x},\omega\right) \equiv \int d^3k\ (2\pi)^{-3}\widetilde{\delta c}\left(\vec{k},\omega\right)e^{-i\vec{k}\cdot\vec{x}}. \quad \text{[S5]}$$

We first find the power spectrum for r_n, using the fluctuation–dissipation theorem. To do so, we solve Eq. **S1** for $\widetilde{\delta c}$ and, using Eq. **S5**, insert it into Eq. **S2** to obtain

$$\{\mu - i\omega[1+\alpha\Sigma(\omega)]\}\widetilde{\delta r}_n - i\omega\alpha\sum_{n'\neq n} V\left(|\vec{x}_n - \vec{x}_{n'}|,\omega\right)\widetilde{\delta r}_{n'} = \alpha\bar{c}_n\widetilde{\delta F}_n, \quad \text{[S6]}$$

where

$$\Sigma(\omega) \equiv \int \frac{d^3k}{(2\pi)^3}\frac{1}{Dk^2 - i\omega} = \frac{1}{2\pi^2}\int_0^\infty dk\,\frac{k^2}{Dk^2 - i\omega} \quad \text{[S7]}$$

and

$$V(x,\omega) \equiv \int \frac{d^3k}{(2\pi)^3}\frac{e^{-i\vec{k}\cdot\vec{x}}}{Dk^2 - i\omega} = \frac{1}{2\pi^2 x}\int_0^\infty dk\,\frac{k\sin(kx)}{Dk^2 - i\omega} \quad \text{[S8]}$$

are the "self-energy" and "interaction potential" between cells mediated by diffusion, respectively (14). The simplifications in Eqs. **S7** and **S8** come from writing the volume element $d^3k = k^2\sin\theta\, dk\, d\theta\, d\phi$ in spherical coordinates aligned with $\vec{x}$, such that $\vec{k}\cdot\vec{x} = k\,x\cos\theta$.

We are interested in the low-frequency limits of $\Sigma(\omega)$ and $V(x,\omega)$. $V(x,0) = 1/(4\pi Dx)$ is finite, whereas $\Sigma(0)$ diverges. The divergence stems from the delta functions in the dynamical equations, which model the cells as point sources. As in ref. 14, we regularize the divergence by introducing a cutoff $\Lambda \sim \pi/a$ at large k to account for the fact that cells have finite extent a, making $\Sigma(0) \sim (2\pi^2)^{-1}\int_0^\Lambda dk/D = 1/(2\pi aD)$. This models cells as spheres of diameter a, but the exact shape of the cell will not be important for the limits we take. These expressions allow us to write Eq. **S6** as

$$\sum_{n'=1}^{N} L_{nn'}\widetilde{\delta r}_{n'} = \frac{\alpha\bar{c}_n}{\mu}(1+i\omega\tau_1)\widetilde{\delta F}_n, \quad \text{[S9]}$$

where

$$\tau_1 \equiv \frac{1}{\mu} + \frac{\alpha/\mu}{2\pi a\, D}, \quad \text{[S10]}$$

$$L_{nn'} \equiv \delta_{nn'} + \frac{z(1-\delta_{nn'})}{|n-n'|}, \quad \text{[S11]}$$

$$z \equiv -i\omega\frac{\alpha/\mu}{4\pi a\, D}. \quad \text{[S12]}$$

In writing Eq. **S9**, we have assumed that $\omega\tau_1$ is small. This assumption is valid for integration times $T = 2\pi/\omega$ much longer than τ_1; we support this assumption in Discussion in the main text. The quantity τ_1 is the receptor equilibration time: it is the time it takes for a signal molecule to unbind from the receptors and diffuse away from the cell into the bulk (27). Its first term μ^{-1} is the intrinsic receptor unbinding time, and its second term $K/4\pi\sigma D$ (where $K = \alpha/\mu$ is the equilibrium constant and $\sigma = a/2$ is the cell radius) accounts for rebinding events that occur before the molecule diffuses away from the cell completely (25). Either term can dominate: The first term dominates if the intrinsic association rate α is much smaller than the diffusion-limited association rate $4\pi\sigma D$, because then the molecule rarely rebinds. Conversely, the second term dominates if α is much larger than $4\pi\sigma D$, because then rebinding is frequent and comprises most of the escape time. We see from Eqs. **S10** and **S12** that $|z| < \omega\tau_1$; therefore, we also treat z as a small parameter.

Solving Eq. **S9** for $\widetilde{\delta r}_n$ requires inverting the matrix $L_{nn'}$. This matrix is a Toeplitz matrix (a matrix with constant diagonals), which has a known inversion algorithm (26). Because $L_{nn'}$ is also symmetric, it is completely specified by its first row $[1\ \rho_1\ \rho_2\ \ldots\ \rho_{N-1}]$. The inversion is performed recursively as follows. First, one introduces $N-1$ scalars $h_1, h_2, \ldots, h_{N-1}$ and $N-1$ column vectors $\vec{q}^{(1)}, \vec{q}^{(2)}, \ldots, \vec{q}^{(N-1)}$. These are initialized as

$$h_1 = 1 - (\rho_1)^2, \quad \vec{q}^{(1)} = [-\rho_1], \quad \text{[S13]}$$

and updated as

$$h_{k+1} = h_k - \frac{(\zeta_k)^2}{h_k}, \quad \vec{q}^{(k+1)} = \begin{bmatrix} \vec{q}^{(k)} - \zeta_k\widehat{\vec{q}}^{(k)}/h_k \\ -\zeta_k/h_k \end{bmatrix}, \quad \text{[S14]}$$

where $\zeta_k \equiv \rho_{k+1} + \sum_{\ell=1}^{k}\rho_\ell\hat{q}_\ell^{(k)}$, and $\widehat{\vec{q}}$ is $\vec{q}$ with the elements in reverse order. Then the inverse is written in terms of the final quantities $h_{N-1} \equiv H$ and $\vec{q}^{(N-1)} \equiv \vec{Q}$. The upper left element is

$$L_{11}^{-1} = \frac{1}{H}, \quad \text{[S15]}$$

the rest of the first row and the column are

$$L_{i+1,1}^{-1} = L_{1,i+1}^{-1} = \frac{Q_i}{H} \quad (1 \le i \le N-1), \quad \text{[S16]}$$

and the diagonals are calculated recursively from the first row and column as

$$L_{i+1,j+1}^{-1} = L_{ij}^{-1} + \frac{(Q_iQ_j - \hat{Q}_i\hat{Q}_j)}{H} \quad (1 \le \{i,j\} \le N-1). \quad \text{[S17]}$$

We now apply this algorithm to Eq. **S11**, keeping only terms up to first order in the small quantity z. From Eq. **S11** we have $\rho_j = z/j$. The initial values are

$$h_1 = 1 - z^2 \approx 1, \quad \vec{q}^{(1)} = [-z]. \tag{S18}$$

Using $\zeta_1 = z/2 + (z)(z) \approx z/2$, the first recursive step gives

$$h_2 = 1 - \frac{(z/2)^2}{1} \approx 1, \quad \vec{q}^{(2)} = \begin{bmatrix} -z - (z/2)(-z)/(1) \\ -(z/2)/(1) \end{bmatrix} \approx \begin{bmatrix} -z \\ -z/2 \end{bmatrix}. \tag{S19}$$

Continuing the recursion establishes the general formulas

$$h_k = 1, \quad \vec{q}_j^{(k)} = \frac{-z}{j} \quad (j \le k), \tag{S20}$$

from which we extract the final values,

$$H = 1, \quad Q_j = \frac{-z}{j}. \tag{S21}$$

These values immediately provide the first row and column of the inverse according to Eqs. **S15** and **S16**. Then noting that the second term on the right-hand side of Eq. **S17** is second order in z, that equation implies that the diagonals of the inverse are constant. We therefore have the inverse to first order in z,

$$L^{-1}_{nn'} = \delta_{nn'} - \frac{z(1-\delta_{nn'})}{|n-n'|}. \tag{S22}$$

The inverse allows us to solve Eq. **S9** for $\widetilde{\delta r}_n$,

$$\widetilde{\delta r}_n = \sum_{n'=1}^{N} G_{nn'} \widetilde{\delta F}_{n'}, \tag{S23}$$

where

$$G_{nn'}(\omega) = \frac{\alpha}{\mu}(1 + i\omega\tau_1) L^{-1}_{nn'} \bar{c}_{n'} = \begin{cases} \dfrac{\alpha \bar{c}_n}{\mu}\left[1 + i\dfrac{\omega}{\mu}\left(1 + \dfrac{\alpha}{2\pi a D}\right)\right] & n' = n, \\ \dfrac{\alpha^2 \omega \bar{c}_{n'}}{4\pi a D \mu^2 |n-n'|}\left[i - \dfrac{\omega}{\mu}\left(1 + \dfrac{\alpha}{2\pi a D}\right)\right] & n' \neq n, \end{cases} \tag{S24}$$

is the generalized susceptibility. The fluctuation–dissipation theorem then gives the power spectrum,

$$S^{rr}_{nn'}(\omega) = \frac{2}{\omega}\mathrm{Im}\,[G_{nn'}(\omega)] = \frac{2\alpha \bar{c}_{n'}}{\mu^2} \begin{cases} \left(1 + \dfrac{\alpha}{2\pi a D}\right) & n' = n, \\ \dfrac{\alpha}{4\pi a D} \dfrac{1}{|n-n'|} & n' \neq n, \end{cases} \tag{S25}$$

as in Eq. **9** of the main text.

We now solve for the power spectra for x_N and y_N. Using Eqs. **S3** and **S4**, we obtain

$$S^{xx}_{NN}(\omega) = \left\langle \widetilde{\delta x}^*_N \widetilde{\delta x}_N \right\rangle = \frac{1}{\nu^2 + \omega^2}\left[\beta^2 S^{rr}_{NN}(\omega) + \left\langle \tilde{\xi}^*_N \tilde{\xi}_N \right\rangle\right], \tag{S26}$$

$$S^{yy}_{NN}(\omega) = \left\langle \widetilde{\delta y}^*_N \widetilde{\delta y}_N \right\rangle = \frac{1}{\nu^2} \sum_{nn'} \tilde{M}^{-1*}_{Nn} \tilde{M}^{-1}_{Nn'} \left[\beta^2 S^{rr}_{nn'}(\omega) + \left\langle \tilde{\chi}^*_n \tilde{\chi}_{n'} \right\rangle\right], \tag{S27}$$

$$S^{xy}_{NN}(\omega) = \left\langle \widetilde{\delta x}^*_N \widetilde{\delta y}_N \right\rangle = \frac{1}{\nu(\nu + i\omega)} \sum_{n} \tilde{M}^{-1}_{Nn} \beta^2 S^{rr}_{Nn}(\omega), \tag{S28}$$

where $\tilde{M}_{nn'} \equiv M_{nn'} - i(\omega/\nu)\delta_{nn'}$. Now taking the low-frequency limit imposes our second timescale assumption, namely $T \gg \tau_2 \equiv 1/\nu$, where τ_2 is the timescale of messenger turnover by degradation. The noise spectra in Eqs. **S26** and **S27** follow directly from Fourier transforming Eq. **4** of the main text and using the steady-state means of Eq. **3** of the main text to eliminate $\beta \bar{r}_n$,

$$\begin{aligned} \left\langle \tilde{\xi}^*_N \tilde{\xi}_N \right\rangle &= 2\nu \bar{x}_N, \\ \left\langle \tilde{\chi}^*_n \tilde{\chi}_{n'} \right\rangle &= \nu(M_{nn'} \bar{y}_{n'} + M_{n'n} \bar{y}_n). \end{aligned} \tag{S29}$$

The appearance of $M_{nn'}$ in Eq. **S29** is expected, because the noise arises in reactions in every cell and then propagates to other cells via the same matrix as the means (28). Indeed, this simplifies Eq. **S27** for $\omega \to 0$, because then $M_{nn'} = \tilde{M}_{nn'}(\omega = 0)$ hits its own inverse. The result is an expression for the variance,

$$(\delta\Delta_N)^2 = (\delta x_N)^2 + (\delta y_N)^2 - 2C^{xy}_{NN} \tag{S30}$$

$$= \frac{1}{T}\left[S^{xx}_{NN}(0) + S^{yy}_{NN}(0) - 2S^{xy}_{NN}(0)\right] \tag{S31}$$

$$= \frac{\beta^2}{\nu^2}\left[\frac{S^{rr}_{NN}(0)}{T} + \sum_{nn'} K_{N-n} K_{N-n'} \frac{S^{rr}_{nn'}(0)}{T} - 2\sum_{n} K_{N-n} \frac{S^{rr}_{Nn}(0)}{T}\right] + \frac{2}{\nu T}(\bar{x}_N + K_0 \bar{y}_N), \tag{S32}$$

as in Eq. **10** of the main text.

SNR in the Many-Cell, Strong-Communication Limit

The variance of the readout is given by Eq. **10** of the main text,

$$(\delta\Delta_N)^2 = \frac{\beta^2}{\nu^2}\left[\frac{S^{rr}_{NN}(0)}{T} + \sum_{n,n'=1}^{N} K_{N-n}\, K_{N-n'} \frac{S^{rr}_{nn'}(0)}{T} - 2\sum_{n=1}^{N} K_{N-n} \frac{S^{rr}_{Nn}(0)}{T}\right] + \frac{2}{\nu T}(\bar{x}_N + K_0 \bar{y}_N), \tag{S33}$$

where $\bar{x}_N = \alpha\beta \bar{c}_N/\mu\nu$ and $\bar{y}_N = \alpha\beta \sum_{n=0}^{N-1} K_n \bar{c}_{N-n}/\mu\nu$. In the limit of many cells ($N \gg 1$) and strong communication ($\gamma \gg \nu$), the kernel takes the approximate form

$$K_n \approx \frac{1}{n_0} e^{-n/n_0}, \tag{S34}$$

where $n_0 \equiv \sqrt{\gamma/\nu} \gg 1$ is the communication length scale (4). Using Eqs. **S25** and **S34**, we evaluate Eq. **S33** term by term.

The first, fourth, and fifth terms in Eq. **S33** are straightforward,

$$\frac{\beta^2}{\nu^2}\frac{S^{rr}_{NN}(0)}{T} = \frac{2}{\mu T}\frac{\alpha\beta^2}{\mu\nu^2}\bar{c}_N + \frac{1}{\pi a D T}\frac{\alpha^2\beta^2}{\mu^2\nu^2}\bar{c}_N, \tag{S35}$$

$$\frac{2}{\nu T}\bar{x}_N = \frac{2}{\nu T}\frac{\alpha\beta}{\mu\nu}\bar{c}_N, \tag{S36}$$

$$\frac{2}{\nu T}K_0\bar{y}_N = \frac{2}{\nu T}\frac{\alpha\beta}{\mu\nu}\frac{\bar{c}_{N-n_0}}{n_0}. \tag{S37}$$

In the last equation we use the limit of large N to approximate the sum in $\bar{y}_N$ as an integral,

$$\sum_{n=0}^{N-1} K_n \bar{c}_{N-n} \approx \int_0^\infty dn\, \frac{1}{n_0} e^{-n/n_0}(\bar{c}_N - nag) = \bar{c}_N - n_0 ag = \bar{c}_{N-n_0}. \tag{S38}$$

The third term in Eq. **S33** we split in two,

$$-2\frac{\beta^2}{\nu^2}\sum_{n=1}^{N} K_{N-n}\frac{S^{rr}_{Nn}(0)}{T} = -2\frac{\beta^2}{\nu^2}\left[K_0\frac{S^{rr}_{NN}(0)}{T} + \sum_{n=1}^{N-1} K_{N-n}\frac{S^{rr}_{Nn}(0)}{T}\right]. \tag{S39}$$

The first of these is like Eq. **S35**,

$$-2\frac{\beta^2}{\nu^2}K_0\frac{S^{rr}_{NN}(0)}{T} = -\frac{4}{\mu T}\frac{\alpha\beta^2}{\mu\nu^2}\frac{\bar{c}_N}{n_0} - \frac{2}{\pi aDT}\frac{\alpha^2\beta^2}{\mu^2\nu^2}\frac{\bar{c}_N}{n_0}. \tag{S40}$$

The second one evaluates to

$$-2\frac{\beta^2}{\nu^2}\sum_{n=1}^{N-1} K_{N-n}\frac{S^{rr}_{Nn}(0)}{T} = -2\frac{\beta^2}{\nu^2}\sum_{n=1}^{N-1}\frac{1}{n_0}e^{-(N-n)/n_0} \times \frac{2\alpha}{\mu^2 T}[\bar{c}_N - (N-n)ag]\frac{\alpha}{4\pi aD}\frac{1}{N-n} \tag{S41}$$

$$= -\frac{1}{\pi aDT}\frac{\alpha^2\beta^2}{\mu^2\nu^2}\left[\frac{\bar{c}_N}{n_0}\sum_{j=1}^{N-1}\frac{e^{-j/n_0}}{j} - \frac{ag}{n_0}\sum_{j=1}^{N-1} e^{-j/n_0}\right] \tag{S42}$$

$$\approx -\frac{1}{\pi aDT}\frac{\alpha^2\beta^2}{\mu^2\nu^2}\left[\frac{\bar{c}_N}{n_0}\log n_0 - ag\right], \tag{S43}$$

where the last step again uses the integral approximation for large N. In particular, we have written

$$\sum_{j=1}^{N-1}\frac{e^{-j/n_0}}{j} \approx \frac{1}{2}e^{-1/n_0} + \int_1^\infty dj\,\frac{e^{-j/n_0}}{j} \tag{S44}$$

$$= \frac{1}{2}\left(1 + \sum_{\ell=1}^{\infty}\frac{(-1/n_0)^\ell}{\ell!}\right) + \log n_0 - \gamma_e - \sum_{k=1}^{\infty}\frac{(-1/n_0)^k}{k!k} \tag{S45}$$

$$\approx \log n_0, \tag{S46}$$

where the first step uses the Euler–Maclaurin formula (ignoring higher-order corrections and taking $N\to\infty$), the second step expands the exponential and replaces the integral form of the upper incomplete Gamma function with its explicit sum, and the last step neglects terms of order $1/n_0$ and assumes $\log n_0 \gg (\gamma_e - 1/2) \approx 0.077$ for the Euler–Mascheroni constant γ_e. Numerically, we have checked that Eq. **S46** is valid for $3 \lesssim n_0 \ll N$, with the error only ~10% for the smallest n_0. This ensures that the derived bounds are applicable in the context of realistic biological systems, such as mammary epithelial organoids (4). Altogether, the third term in Eq. **S33** is then

$$-2\frac{\beta^2}{\nu^2}\sum_{n=1}^{N} K_{N-n}\frac{S^{rr}_{Nn}(0)}{T} = -\frac{4}{\mu T}\frac{\alpha\beta^2}{\mu\nu^2}\frac{\bar{c}_N}{n_0} - \frac{2}{\pi aDT}\frac{\alpha^2\beta^2}{\mu^2\nu^2}\left[\frac{\bar{c}_N}{n_0} + \frac{\bar{c}_N}{2n_0}\log n_0 - \frac{ag}{2}\right] \tag{S47}$$

$$\approx -\frac{4}{\mu T}\frac{\alpha\beta^2}{\mu\nu^2}\frac{\bar{c}_N}{n_0} - \frac{2}{\pi aDT}\frac{\alpha^2\beta^2}{\mu^2\nu^2}\frac{\log n_0}{2n_0}\bar{c}_N, \tag{S48}$$

where the second step uses $\bar{c}_N - agn_0/2 = \bar{c}_{N-n_0/2} < \bar{c}_N$ and assumes $\log n_0 \gg 2$.

The second term in Eq. **S33** we also split in two,

$$\frac{\beta^2}{\nu^2}\sum_{n,n'=1}^{N} K_{N-n}\,K_{N-n'}\frac{S^{rr}_{nn'}(0)}{T} = \frac{\beta^2}{\nu^2}\left[\sum_{n=1}^{N} K^2_{N-n}\frac{S^{rr}_{nn}(0)}{T} + \sum_{n=1}^{N}\sum_{n'\neq n} K_{N-n}\,K_{N-n'}\frac{S^{rr}_{nn'}(0)}{T}\right]. \tag{S49}$$

The first of these is straightforward to evaluate with the integral approximation in Eq. **S38**,

$$\frac{\beta^2}{\nu^2}\sum_{n=1}^{N} K^2_{N-n}\frac{S^{rr}_{nn}(0)}{T} = \frac{\beta^2}{\nu^2}\sum_{j=0}^{N-1}\frac{1}{n_0^2}e^{-2j/n_0}\frac{2\alpha\bar{c}_{N-j}}{\mu^2 T}\left(1 + \frac{\alpha}{2\pi aD}\right) \tag{S50}$$

$$\approx \frac{2}{\mu T}\frac{\alpha\beta^2}{\mu\nu^2}\frac{\bar{c}_{N-n_0/2}}{2n_0} + \frac{1}{\pi aDT}\frac{\alpha^2\beta^2}{\mu^2\nu^2}\frac{\bar{c}_{N-n_0/2}}{2n_0}. \tag{S51}$$

The second can be evaluated in two parts,

$$\frac{\beta^2}{\nu^2}\sum_{n=1}^{N}\sum_{n'\neq n} K_{N-n}\,K_{N-n'}\frac{S^{rr}_{nn'}(0)}{T} = \frac{1}{2\pi aDT}\frac{\alpha^2\beta^2}{\mu^2\nu^2} \times \left[\frac{\bar{c}_N}{n_0^2}\underbrace{\sum_{j=0}^{N-1}\sum_{j'\neq j}\frac{e^{-(j+j')/n_0}}{|j-j'|}}_{A} - \frac{ag}{n_0^2}\underbrace{\sum_{j=0}^{N-1}\sum_{j'\neq j}\frac{j' e^{-(j+j')/n_0}}{|j-j'|}}_{B}\right]. \tag{S52}$$

Note that $B = -\partial_u A/2$, where $u \equiv 1/n_0$, so that we need only to evaluate A. We split A into two equal components,

$$= \sum_{j=0}^{N-1}\sum_{j'=0}^{j-1}\frac{e^{-(j+j')/n_0}}{j-j'} + \sum_{j=0}^{N-1}\sum_{j'=j+1}^{N-1}\frac{e^{-(j+j')/n_0}}{j'-j} \tag{S53}$$

$$= 2\sum_{j=0}^{N-1}\sum_{j'=0}^{j-1}\frac{e^{-(j+j')/n_0}}{j-j'}, \tag{S54}$$

and rewrite it in terms of $k = j + j'$ and $\ell = j - j'$,

$$A = 2\sum_{\ell=1}^{N-1}\sum_{k=\ell,\,\ell+2,\,\ell+4,\,\ldots}^{2(N-1)-\ell}\frac{e^{-k/n_0}}{\ell}. \qquad \textbf{[S55]}$$

We approximate with integrals for large N, accounting for the fact that k has support on only half of the integers in its range,

$$A \approx 2\int_1^N d\ell\,\frac{1}{2}\int_\ell^{2(N-1)-\ell} dk\,\frac{e^{-k/n_0}}{\ell} \qquad \textbf{[S56]}$$

$$= n_0\int_1^N d\ell\,\frac{e^{-\ell/n_0}}{\ell} - n_0 e^{-2N}\int_1^N d\ell\,\frac{e^{\ell/n_0}}{\ell}. \qquad \textbf{[S57]}$$

The first integral is approximately $\log n_0$ by Eq. **S46**. The second integral evaluates to $\mathrm{Ei}(N/n_0) - \mathrm{Ei}(1/n_0)$, where Ei is the exponential integral function, whose large- and small-argument limits are $\mathrm{Ei}(N/n_0) \approx e^{N/n_0}/(N/n_0)$ and $\mathrm{Ei}(1/n_0) \approx -\log n_0$, respectively. Thus, the second term in Eq. **S57** vanishes exponentially with N, and we have

$$A = n_0\,\log n_0, \qquad \textbf{[S58]}$$

$$B = \frac{n_0^2}{2}(1+\log n_0) \approx \frac{n_0^2}{2}\log n_0, \qquad \textbf{[S59]}$$

making the term in brackets in Eq. **S52** equal to $(\bar{c}_N - a g n_0/2)(\log n_0)/n_0 = (\bar{c}_{N-n_0/2}\log n_0)/n_0$. Altogether, the second term in Eq. **S33** is then

$$\frac{\beta^2}{\nu^2}\sum_{n,n'=1}^{N} K_{N-n}K_{N-n'}\frac{S^{rr}_{nn'}(0)}{T} = \frac{2}{\mu T}\frac{\alpha\beta^2}{\mu\nu^2}\frac{\bar{c}_{N-n_0/2}}{2n_0} + \frac{1}{\pi a D T}\frac{\alpha^2\beta^2}{\mu^2\nu^2}\left[\frac{\bar{c}_{N-n_0/2}}{2n_0} + \frac{\log n_0}{2n_0}\bar{c}_{N-n_0/2}\right] \qquad \textbf{[S60]}$$

$$\approx \frac{2}{\mu T}\frac{\alpha\beta^2}{\mu\nu^2}\frac{\bar{c}_{N-n_0/2}}{2n_0} + \frac{1}{\pi a D T}\frac{\alpha^2\beta^2}{\mu^2\nu^2}\frac{\log n_0}{2n_0}\bar{c}_{N-n_0/2}, \qquad \textbf{[S61]}$$

where the second step assumes $\log n_0 \gg 1$.

Finally, collecting the terms in Eqs. **S35–S37**, **S48**, and **S61**, the variance in Eq. **S33** becomes

$$(\delta\Delta_N)^2 = \left(\frac{\alpha\beta}{a^3\mu\nu}\right)^2\Bigg[\underbrace{\frac{a^2}{\pi D T}\left(\bar{c}_N + \frac{\log n_0}{2n_0}\bar{c}_{N-n_0/2} - 2\frac{\log n_0}{2n_0}\bar{c}_N\right)a^3}_{\textbf{Extrinsic} \text{ noise from } c, \text{ propagated to } x \text{ and } y} + \underbrace{\frac{2}{\mu T}\frac{a^3\mu}{\alpha}\left(\bar{c}_N + \frac{\bar{c}_{N-n_0/2}}{2n_0} - 2\frac{\bar{c}_N}{n_0}\right)a^3}_{\textbf{Intrinsic} \text{ noise in } r, \text{ propagated to } x \text{ and } y} + \underbrace{\frac{2}{\nu T}\frac{a^3\mu}{\alpha}\frac{\nu}{\beta}(\bar{c}_N)a^3}_{\textbf{Intrinsic} \text{ noise in } x} + \underbrace{\frac{2}{\nu T}\frac{a^3\mu}{\alpha}\frac{\nu}{\beta}\left(\frac{\bar{c}_{N-n_0}}{n_0}\right)a^3}_{\textbf{Intrinsic} \text{ noise in } y}\Bigg]. \qquad \textbf{[S62]}$$

The last line contains the intrinsic noise from x_N and y_N. For example, the first term in this line is $(\delta x_N)^2 = (2/\nu T)(\alpha\beta\bar{c}_N/\mu\nu) = 2\bar{x}_N/\nu T$; the relative noise $(\delta x_N/\bar{x}_N)^2 = 2/\nu T\bar{x}_N$ then decreases with the number of molecules $\bar{x}_N \times \nu T$ that are turned over in time T, as expected for intrinsic counting noise. The second term in this line is for y and is similar, except that because the global species is exchanged over roughly n_0 cells, more molecules are counted and the noise is reduced by a factor n_0. The second line contains the intrinsic noise in r, propagated to x and y. The third line contains the noise in c, propagated to x and y, which we deem extrinsic, because it originates in the environment and is not under direct control of the cells.

Importantly, the intrinsic noise terms in Eq. **S62** are reducible by increasing the numbers of receptors and local and global species molecules. These molecule numbers are set by the gain factors $\bar{r}_N/a^3\bar{c}_N = \alpha/a^3\mu$ and $\bar{x}_N/\bar{r}_N = \beta/\nu$, and indeed, we see that the second and third lines in Eq. **S62** vanish as the gain factors grow large. In this limit we are left with only the lower bound set by the extrinsic noise,

$$(\delta\Delta_N)^2 \geq \left(\frac{\alpha\beta}{\mu\nu}\right)^2\frac{1}{\pi a D T}\left(\bar{c}_N + \frac{\log n_0}{2n_0}\bar{c}_{N-n_0/2} - 2\frac{\log n_0}{2n_0}\bar{c}_N\right). \qquad \textbf{[S63]}$$

Dividing by the square of the mean $\bar{\Delta}_N = \alpha\beta n_0 a g/\mu\nu$ produces Eqs. **11** and **12** in the main text.

Exact SNR for Regional Excitation–Global Inhibition

In the regional excitation–global inhibition (REGI) strategy, both messengers X and Y are exchanged between cells, at rates γ_x and γ_y, respectively. This results in a straightforward generalization of the expression for the signal-to-noise ratio (SNR). Specifically, the mean becomes (compare with Eqs. **5** and **6** in the main text)

$$\bar{\Delta}_N = \frac{\alpha\beta}{\mu\nu}\left(\sum_{n=0}^{N-1}K^x_n\bar{c}_{N-n} - \sum_{n=0}^{N-1}K^y_n\bar{c}_{N-n}\right), \qquad \textbf{[S64]}$$

where now there are two communication kernels,

$$K^x_n = \frac{\sum_{j=0}^{N-n-1}\binom{N-n-1+j}{2j}(\nu/\gamma_x)^j}{\sum_{\ell=0}^{N-1}\binom{N+\ell}{2\ell+1}(\nu/\gamma_x)^\ell}, \qquad \textbf{[S65]}$$

$$K^y_n = \frac{\sum_{j=0}^{N-n-1}\binom{N-n-1+j}{2j}(\nu/\gamma_y)^j}{\sum_{\ell=0}^{N-1}\binom{N+\ell}{2\ell+1}(\nu/\gamma_y)^\ell}. \qquad \textbf{[S66]}$$

The variance becomes (compare with Eq. **10** in the main text)

$$(\delta\Delta_N)^2 = \frac{\beta^2}{\nu^2}\left[\sum_{nn'}\left(K^x_{N-n}K^x_{N-n'} + K^y_{N-n}K^y_{N-n'} - 2K^x_{N-n}K^y_{N-n'}\right)\frac{S^{rr}_{nn'}(0)}{T}\right] + \frac{2}{\nu T}\left(K^x_0\bar{x}_N + K^y_0\bar{y}_N\right), \qquad \textbf{[S67]}$$

where the bound receptor power spectrum $S^{rr}_{nn'}(\omega)$ remains the same as in Eq. **9** in the main text (or equivalently Eq. **S25** here). The SNR is then $(\bar{\Delta}_N/\delta\Delta_N)^2$.

The SNR has a maximum as a function of the rate ratio γ_x/γ_y. The location of the maximum γ_x^*/γ_y must lie between 0 and 1. At $\gamma_x/\gamma_y = 0$, the X messenger is not exchanged, and we recover the SNR of the local excitation–global inhibition (LEGI) strategy, which is a limiting case of REGI. At $\gamma_x/\gamma_y = 1$, there is no difference between X and Y, and the signal (and therefore the SNR) is 0. The exact location of γ_x^*/γ_y depends on factors that are specific to the system, e.g., the concentration profile $\bar{c}_n$, the environmental and system parameters, and the measurement location ($n = 1$ vs. $n = N$).

We illustrate the dependence of γ_x^*/γ_y on particular system parameters, namely the gain factors $\alpha/a^3\mu$ and β/ν. For this, Fig. S1 shows the dependence of the SNR on γ_x/γ_y as we vary the gain factors $\alpha/a^3\mu$ (Fig. S1*A*) and β/ν (Fig. S1*B*). In both cases, we see that the optimal rate ratio γ_x^*/γ_y increases with increasing gain. This is because increasing either gain factor increases the number of internal messenger molecules. With more molecules, the system can afford to increase γ_x while maintaining the same difference in molecule number Δ_N in the Nth cell. The increase in γ_x enhances the spatial averaging by the X messenger and thus reduces the noise in the estimate of $\bar{c}_N$. Therefore, we see in Fig. S1 that the maximal SNR occurs at a higher γ_x^* value as either gain is increased.

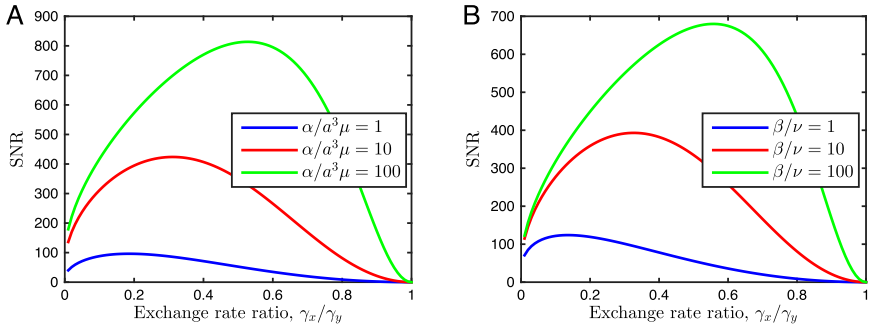

Fig. S1. Dependence of the optimal exchange rate ratio on system parameters in the regional excitation–global inhibition (REGI) strategy. The signal-to-noise ratio (SNR) has a maximum at a particular rate ratio γ_x^*/γ_y, which increases as a function of either gain factor, (*A*) $\alpha/a^3\mu$ or (*B*) β/ν. Parameters are $a = 10$ μm, $\bar{c}_N = 1$ nM, $g = 1$ nM/mm, $D = 50$ μm^2/s, $T = 10$ s, $\mu = \nu = 1$ s^{-1}, $N = 100$, and $n_y = \sqrt{\gamma/\nu} = 10$. In *A*, $\beta/\nu = 5$, and $\alpha/a^3\mu$ is varied as indicated. In *B*, $\alpha/a^3\mu = 5$, and β/ν is varied as indicated.